Quantum mechanical calculations of rotational–vibrational scattering in homonuclear diatom–atom collisions

Albert F. Wagner and Vincent McKoy*

Arthur Amos Noyes Laboratory of Chemical Physics,† California Institute of Technology, Pasadena, California 91109

(Received 10 September 1971)

Most calculations of the vibrational scattering of diatom–atom collisions use the breathing sphere approximation (BSA) of orientation averaging the intermolecular potential. The resulting angularly symmetric potential can not cause rotational scattering. We determine the error introduced by the BSA into observables of the vibrational scattering of low-energy homonuclear diatom–atom collisions by comparing two quantum mechanical calculations, one with the BSA and the other with the full angularly asymmetric intermolecular potential. For reasons of economy the rotational scattering of the second calculation is restricted by the use of special incomplete channel sets in the expansion of the scattering wavefunction. Three representative collision systems are studied: H_2–Ar, O_2–He, and I_2–He. From our calculations, we reach two conclusions. First, the BSA can be used to analyze accurately experimental measurements of vibrational scattering. Second, measurements most sensitive to the symmetric part of the intermolecular potential are, in order, elastic cross sections, inelastic cross sections, and inelastic differential cross sections. Elastic differential cross sections are sensitive to the potential only if the collision is "sticky," with scattering over a wide range of angles; I_2–He is such a collision. Otherwise the potential sensitivity of elastic differential cross sections is concentrated in the experimentally difficult region of very small angle scattering.

I. INTRODUCTION

The study of intermolecular forces is a major motivation for many experiments in nonreactive, vibrationally inelastic diatom–atom collisions.[1] In these collisions, the most detailed observation possible has the form $O_{\alpha' l_1' m_1'}^{\alpha l_1 m_1}$. This designates an observation of the scattering from initial diatomic state $|\alpha' l_1' m_1'\rangle$ to final state $|\alpha l_1 m_1\rangle$. Here and elsewhere α and l_1 are the diatom's vibrational and rotational quantum numbers and m_1 is the diatom's angular momentum projection quantum number along the initial direction of the atom. A primed quantum number shows that it indexes the precollision system. In most experiments the diatom is not prepared in a specific rotational state and is randomly oriented. Also, the diatom's rotational state and orientation after scattering is not resolved. In such experiments, the only observation possible has the form $O_{\alpha'}^{\alpha}$, designating an observation of the scattering from one diatom vibrational state to another.

An intermolecular potential (IP) can be quantitatively determined only when experimental measurements can be reproduced by a calculation with an assumed IP. Therefore, one needs to calculate at least $O_{\alpha'}^{\alpha}$. $O_{\alpha'}^{\alpha}$ can not be directly calculated, because it obeys the relation

$$O_{\alpha'}^{\alpha} = \sum_{l_1'} P_{\alpha'}(l_1') O_{\alpha' l_1'}^{\alpha}, \tag{1}$$

where $P_{\alpha'}(l_1')$ is the experimentally controlled probability that the diatom with quantum number α' will also have quantum number l_1'. $O_{\alpha' l_1'}^{\alpha}$, which can be calculated, is an observation of the scattering of a randomly oriented diatom in the vibrational rotational state of α' and l_1' into all states with quantum number α. Ideally, the calculation should be quantum mechanical and the assumed IP should be angularly asymmetric so as to cause both rotational and vibrational scattering. However all exact, and most approximate, quantum mechanical calculations[2] of $O_{\alpha' l_1'}^{\alpha}$ use an angularly symmetric IP. Such an approximate IP treats the diatom as a breathing sphere and hence there can be no rotational scattering. There are two reasons for the breathing sphere approximation (BSA). First, $O_{\alpha' l_1'}^{\alpha}$ is mainly a measure of vibrational scattering and so should be sensitive primarily to the symmetric part of the real IP. Second, the wavefunction for a symmetric IP has only enough detail to determine $O_{\alpha' l_1'}^{\alpha}$; but the wavefunction for a realistic IP should determine all $O_{\alpha' l_1' m_1'}^{\alpha l_1 m_1}$ from which $O_{\alpha' l_1'}^{\alpha}$ can be obtained,

$$O_{\alpha' l_1'}^{\alpha} = (2l_1'+1)^{-1} \sum_{m_1'=-l_1'}^{l_1'} \sum_{m_1=-l_1}^{l_1} O_{\alpha' l_1' m_1'}^{\alpha l_1 m_1}. \tag{2}$$

Since each vibrational quantum number indexes tens to hundreds of diatomic states, such information is basically too difficult and expensive to obtain. The approximate quantum mechanical calculations not using the BSA have used instead dynamical approximations that are hard to evaluate. This can be said of most semiclassical and classical calculations[2] not using the BSA. However, a two-dimensional classical calculation by Benson and Berend[3] indicates that the BSA is accurate for the calculation of vibrational relaxation times of O_2–Ar, while a three-dimensional classical calculation by Razner[4] implies that the BSA is inaccurate for the calculation of energy transfer in very energetic Br_2–Ar collisions.

We have been able to determine the degree of error in a BSA calculation of $O_{\alpha' l_1'}^{\alpha}$ for the simplest class of collisions exhibiting vibrational inelasticity—the collision of an atom with a homonuclear diatom at energies low enough to involve only two vibrational states. This is done by comparing two quantum mechanical cal-

culations, one using the BSA and the other an angularly asymmetric IP with restricted rotational scattering. In the next section, we define our coordinate system, units, and the three representative homonuclear diatom–atom collision systems studied: H_2–Ar, O_2–He, and I_2–He. In the third section, we derive the theory for model restricted rotational scattering by a realistic IP. In the fourth section, we discuss the numerical and analytical methods used to solve Schrödinger's equation for the collision system wavefunction. In the fifth section, we study in detail the BSA induced inaccuracies in the partial, and partial differential, cross sections of H_2–Ar. In the sixth section, we study the BSA-induced inaccuracies in the partial cross sections of O_2–He and I_2–He. We then summarize our results.

II. SYSTEM DESCRIPTIONS

Figure 1 shows our coordinate system. Vector $\mathbf{r}_1$ (r_1, θ_1, ϕ_1) is the distance of one end of the diatom from its center of mass and vector $\mathbf{r}_2$ (r_2, θ_2, ϕ_2) is the distance of the colliding atom from the diatom's center of mass. γ is the angle between these two vectors, while the z axis, from which θ_1 and θ_2 are measured, points in the initial direction of the atom.

We represent the diatom as a rigidly rotating harmonic oscillator, an approximation which is valid at our low collision energies. For an IP, we choose

$$V(r_1, r_2, \gamma) = V_0(r_1, r_2) + V_2(r_1, r_2) P_2(\cos\gamma), \quad (3)$$

where

$$V_0(r_1, r_2) = 4\epsilon\{[\sigma/(r_2 - r_1)]^{12} - [\sigma/(r_2 - r_1)]^6\},$$

$$V_2(r_1, r_2) = 4\epsilon\{[\sigma/(r_2 - r_1)]^{12} a_{sr} - [\sigma/(r_2 - r_1)]^6 a_{lr}\},$$

where $P_2(\cos\gamma)$ is the second Legendre polynomial. Both V_0 and V_2 are of a Lennard-Jones type with V_2 modified by a short- and long-range $P_2(\cos\gamma)$ asymmetry defined by a_{sr} and a_{lr}. Real IP's are known[5] to have a long-range attractive and a short-range repulsive part, with each part having its own angular asymmetry; our parametrized IP contains these features.

The Hamiltonian $\mathcal{H}$ for the collision of A striking B_2 is[6]

$$\mathcal{H} = -(2M)^{-1}\nabla_2^2 + [-\tfrac{1}{2}(\partial^2/\partial y^2) + \tfrac{1}{2}y^2 + B_0\hat{L}_1^2] + V(r_1, r_2, \gamma), \quad (4)$$

where

$$M = m_A/(m_A + 2m_B).$$

Here m_A and m_B are the masses of A and B. The units

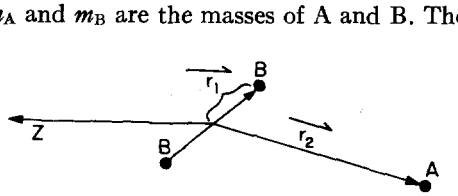

FIG. 1. Coordinates for the collision of atom A with diatom B_2.

TABLE I. System parameters in reduced units.

Parameter	H_2–Ar	O_2–He	I_2–He
M	0.952	0.111	0.0155
B_0	0.0138[a]	0.000918[a]	0.000228[a]
σ	48.14[b]	115.5[c]	128.3[d]
ϵ	0.01158[b]	0.01593[c]	0.4073[d]
a_{sr}	0.25[e]	0.45[f]	0.55[g]
a_{lr}	0.128[h]	0.229[h]	0.10[i]
E	2.140	2.195	2.464
l_1'	3	13	34
T (°K)	2000	800	85

[a] G. Herzberg, *Spectra of Diatomic Molecules* (Van Nostrand, Princeton, N.J., 1950), 2nd ed.

[b] R. Helbing, W. Gaide, and H. Pauly, Z. Physik **208,** 215 (1968).

[c] Derived from the combining laws and the He–He parameters of J. O. Hirschfelder, C. F. Curtiss, and R. B. Bird, *Molecular Theory of Gases and Liquids* (Wiley, New York, 1964), 2nd corrected printing, pp. 168, 1110; and the O_2–O_2 parameters of C. J. G. Raw and C. P. Ellis, J. Chem. Phys. **28,** 1198 (1958).

[d] J. I. Steinfeld and W. Klemperer, J. Chem. Phys. **48,** 3475 (1965); J. I. Steinfeld, J. Phys. Chem. **64,** 14 (1968); parameters are for the $B\,^3\Pi_{0u^+}$ electronic state of I_2.

[e] From the H_2–He potential surface calculated by M. D. Gordon and D. Secrest, J. Chem. Phys. **52,** 120 (1970).

[f] Estimated from the O_2–O_2 atom centered Lennard-Jones potential of J. R. Sweet and W. A. Steele, J. Chem. Phys. **47,** 3029 (1967).

[g] Estimated from the Br_2–Ar atom centered Lennard-Jones potential of R. Razner, J. Chem. Phys. **51,** 5602 (1969).

[h] Derived from the polarization experiments of N. J. Bridge and A. D. Buckingham, Proc. Roy. Soc. (London) **A295,** 334 (1966).

[i] From the value for Br_2–^{7}Li measured by R. K. B. Helbing and E. W. Rothe, J. Chem. Phys. **48,** 3945 (1968).

of energy and length are $\hbar\omega$ and one-half the classical ground state vibrational amplitude, respectively. $\hat{L}_1^2$ is the rotational angular momentum operator, B_0 the rotational constant, and y is the diatom's bond displacement from equilibrium. To specify $\mathcal{H}$ for a collision system we need M, B_0, σ, ϵ, a_{sr}, and a_{lr}.

We considered three systems: H_2–Ar, O_2–He, and I_2–He. The parameters for these three systems are listed in Table I. The IP for H_2–Ar is approximately correct while that for O_2–He is only qualitatively correct. The IP for I_2–He is just a guess, since it is based on results or estimates for a variety of systems. However, for most homonuclear diatom–atom systems realistic values for the six Hamiltonian parameters fall within the range of the values chosen for our three systems. For reasons of economy, each system is studied at one total energy E and one initial rotational state indexed by l_1'. However, each system has different values for these two parameters. E and l_1' are listed in Table I along with T, the temperature equivalent, assuming a Boltzmann

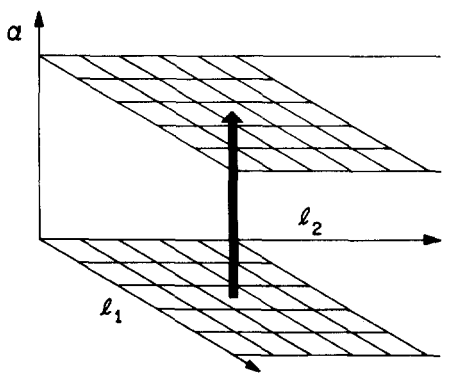

FIG. 2. Channel scattering with an angularly symmetric IP.

distribution, of the relative translational energy of the atom when the total energy is E and the diatom is initially in the l_1' rotational state of the first excited vibrational state. Shock tube experiments on H_2–Ar [7] and O_2–He [8] have been conducted at these temperatures. The value of l_1' for H_2–Ar and O_2–He is not unreasonable for these experiments. At least one experiment on I_2–He [9] has preselected the diatom in our initial rotational state.

III. THEORY

A. Formalism

To determine $O_{\alpha' l_1'}{}^{\alpha}$ for any α we need to know the wavefunction $\psi_{\alpha' l_1' m_1'}{}^{E}$ for all m_1' and the relevant range of E, where

$$\mathcal{H}\psi_{\alpha' l_1' m_1'}{}^{E} = E\psi_{\alpha' l_1' m_1'}{}^{E} \tag{5}$$

and

$$\psi_{\alpha' l_1' m_1'}{}^{E} \underset{r_2\to\infty}{\longrightarrow} |\,\alpha' l_1' m_1'\rangle \exp(i\bar{k}z) + \sum_{\alpha l_1 m_1} f_{\alpha' l_1' m_1'}{}^{\alpha l_1 m_1}(E, \Omega_2)[\exp(ikr_2)/r_2]\,|\,\alpha l_1 m_1\rangle,$$

where $\bar{k}$ and k are the initial and final wavenumbers of the relative motion, $f_{\alpha' l_1' m_1'}{}^{\alpha l_1 m_1}(E, \Omega_2)$ is the amplitude at total energy E for $|\,\alpha' l_1' m_1'\rangle$ to be excited to $|\,\alpha l_1 m_1\rangle$ while scattering the atom into solid angle Ω_2 specified by θ_2 and ϕ_2. $O_{\alpha' l_1'}{}^{\alpha}$ can be determined from all these amplitudes. The usual first step in obtaining $\psi_{\alpha' l_1' m_1'}$ (we will suppress the index E) is its expansion[10] in a set of functions complete in r_1, θ_1, ϕ_1, θ_2, and ϕ_2 space. The spherical harmonics are complete in θ_2 and ϕ_2 space. Furthermore each spherical harmonic describes an orbital angular momentum state of the atom. In the total angular momentum representation the product of the diatomic states, complete in r_1, θ_1, and ϕ_1 space, and the spherical harmonics is the most convenient set of functions to expand $\psi_{\alpha' l_1' m_1'}$. We call a member of that set a channel designated by ${}^{J}|\,\alpha l_1 l_2\rangle$, where l_2 is the orbital quantum number which couples with l_1 to form J, the total angular momentum quantum number. In general, a channel's z component of J should be specified, but atom–diatom scattering is independent of this momentum. A channel is open if its diatomic state factor has an energy less than E; otherwise it is closed.

The boundary condition on $\psi_{\alpha' l_1' m_1'}$ is

$$\psi_{\alpha' l_1' m_1'} \underset{r_2\to\infty}{\longrightarrow} \sum_{l_2'=0} \sum_{J=|l_1'-l_2'|}^{l_1'+l_2'} C_{l_2' J}{}^{\alpha' l_1' m_1'} \left\{ \frac{\exp[-i(\bar{k}r_2 - l_2'\pi/2)]}{k^{1/2} r_2}\, {}^{J}|\,\alpha' l_1' l_2'\rangle - \sum_{\alpha l_1 l_2} {}^{J}S_{\alpha' l_1' l_2'}{}^{\alpha l_1 l_2} \times \frac{\exp[i(kr_2 - l_2\pi/2)]}{k^{1/2} r_2}\, {}^{J}|\,\alpha l_1 l_2\rangle \right\}, \tag{6}$$

where each $C_{l_2' J}{}^{\alpha' l_1' m_1'}$ is a known constant[10] and ${}^{J}S_{\alpha' l_1' l_2'}{}^{\alpha l_1 l_2}$ is an element of what we call a solution vector, ${}^{J}\mathbf{S}_{\alpha' l_1' l_2'}$ in which $O_{\alpha' l_1'}{}^{\alpha}$ can be directly expressed [see Eqs. (7) and (10)]. Let us call the solution to the Schrödinger equation which obeys the boundary condition enclosed in braces above a partial wavefunction (pwfn) designated $\psi_{l_2' J}{}^{\alpha' l_1'}$. $\psi_{l_2' J}{}^{\alpha' l_1'}$ is the wavefunction for that part of the collision system initially described by unit amplitude in ${}^{J}|\,\alpha' l_1' l_2'\rangle$ with unit incoming current in the r_2 direction. The square of ${}^{J}S_{\alpha' l_1' l_2'}{}^{\alpha l_1 l_2}$ is the probability that the collision will scatter ${}^{J}|\,\alpha' l_1' l_2'\rangle$ into ${}^{J}|\,\alpha l_1 l_2\rangle$. To obtain $\psi_{l_2' J}{}^{\alpha' l_1'}$, we expand it in channels and generate a coupled set of differential equations in r_2 for the channel coefficients. The channel coefficients at large r_2 contain the pwfn's solution vector. Describing the collision in terms of the scattering of each initial channel into other channels is more convenient than describing it in terms of the scattering of the initial diatomic state into other states and of the atom into different directions.

B. The Influence of the IP

The expense and difficulty of determining $O_{\alpha' l_1'}{}^{\alpha}$ lie almost entirely in solving the coupled set of differential equations for the channel coefficients of each pwfn. The calculation time for each set is roughly proportional to the number of channel coefficients cubed. The importance of the IP is that a pwfn's channel set is effectively complete if it includes only those channels which the IP significantly couples to the initial channel in some region of r_2. The form of the IP limits a pwfn's channel set in two ways. First, all meaningful IP's must conserve total angular momentum as well as reflect the symmetry of a *homo*nuclear diatom. Therefore, $\psi_{l_2' J}{}^{\alpha' l_1'}$ will need only those channels with total angular momentum J and rotational and orbital angular momenta of the same parity (even or odd) as l_1' and l_2'. Second, if an IP is angularly symmetric, $\psi_{l_2' J}{}^{\alpha' l_1'}$ will need only those channels with rotational and orbital angular momenta l_1' and l_2'. Beyond these two general statements, a pwfn's channel set depends on the strength, not the form, of the IP.

The differences between a BSA and an exact determination of $O_{\alpha' l_1'}{}^{\alpha}$ stem from the differences between the scattering of each initial channel by an angularly symmetric or asymmetric IP. In Figs. 2 and 3 we schematically illustrate the scattering of one initial channel by both IP's. In each figure, a channel is represented by a square whose position specifies the channel's vibrational, rotational, and orbital quantum numbers. Only channels strongly coupled to the initial channel are shown; these channels must have the same J and the same parity in l_1 and l_2 as the initial channel. Arrows of a thickness proportional to the excitation probability connect final and initial channels. For clarity, pure elastic scattering is not shown in either figure and some arrows are left out of Fig. 3. Vibrationally elastic scattering takes place within the initial channel's plane of channels while all other scattering is vibrationally inelastic. Only two channels are coupled in Fig. 2 by the symmetric IP while 50 channels are coupled in Fig. 3 by the asymmetric IP. The ratio of BSA to exact calculation time for the pwfn is therefore $2^3/50^3$ or about 1/16 000. We refer to the scattering between channels alike in l_1 and l_2 as vertical and all other channel scattering as lateral. The symmetric IP causes only vertical scattering, while the asymmetric IP causes both vertical and lateral scattering. The vibrational scattering produced by an elastic or inelastic process is different in at least three ways from that produced by the analogous vertical process. First, the two processes differ in the vibrational coupling between initial and final channels. Second, the energy of rotational and orbital motion during the collision is different; this affects the amount of energy directly available to force vibrational scattering. Third, because the final channels of the two processes differ in l_1 and l_2, they describe an atom–diatom system separating at different speeds in different directions. The greater the change in l_1 and l_2 from l_1' and l_2', the more a lateral process will differ from the analogous vertical one. A pwfn's contribution to $O_{\alpha' l_1'}{}^{\alpha}$ involves a sum over all the vibrationally elastic or inelastic scattering of its initial channel. If, in the exact calculation, the difference between each elastic or inelastic lateral process and the analogous vertical process does not sum to zero for enough initial channels, then the BSA determination of $O_{\alpha' l_1'}{}^{\alpha}$ will be in error.

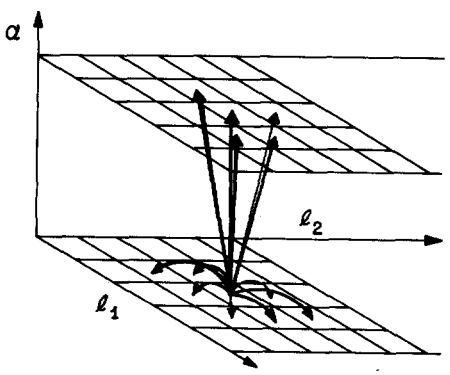

FIG. 3. Channel scattering with an angularly asymmetric IP.

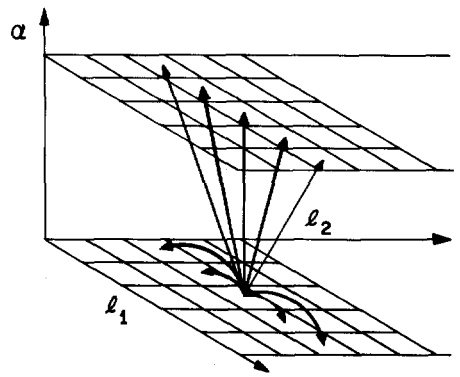

FIG. 4. Channel scattering with an asymmetric IP and an incomplete channel set.

C. Model Rotational Scattering

Suppose we obtain $\psi_{\alpha' l_1' m_1'}$ for an asymmetric IP by expanding each pwfn $\psi_{l_2' J}{}^{\alpha' l_1'}$ in a channel set composed only of channels with l_2 equal to l_2'. This very incomplete channel set does not permit $\psi_{l_2' J}{}^{\alpha' l_1'}$ to obey its boundary condition unless we assume ${}^{J}S_{\alpha' l_1' l_2'}{}^{\alpha l_1 l_2}$ equals zero if l_2 is not equal to l_2'. The channel scattering for the same initial channel of Figs. 2 and 3 is represented in Fig. 4. This calculation takes only 125 times longer than a BSA calculation vs the factor of 16 000 we previously estimated for the exact calculation. However, each lateral scattering process in Fig. 4 is probably more intense than the same process calculated with a complete channel set (Fig. 3) because the initial channel's amplitude is being forced into fewer final channels. This feature implies that differences between lateral and vertical scattering will be larger in the approximate than in the exact calculation. The implication is that the difference between the approximate and the BSA determined $O_{\alpha' l_1'}{}^{\alpha}$ will tend to be larger than the difference between the exact and the BSA determined $O_{\alpha' l_1'}{}^{\alpha}$. Let us define a model calculation of $O_{\alpha' l_1'}{}^{\alpha}$ as one in which each pwfn is expanded in a channel set made incomplete by the same artificial set of restrictions. The degree of error in a BSA $O_{\alpha' l_1'}{}^{\alpha}$ can be semiquantitatively defined by its comparison to $O_{\alpha' l_1'}{}^{\alpha}$ from feasible calculations for models whose restrictions emphasize lateral processes with large changes in l_1 or l_2.

We have studied four different models. We will now define each model's set of restrictions and, as an example, apply these to the pwfn $\psi_{5,5}{}^{0,9}$.

Each model restricts a pwfn's channel set, one plane at a time (see Figs. 2–4), starting from the initial

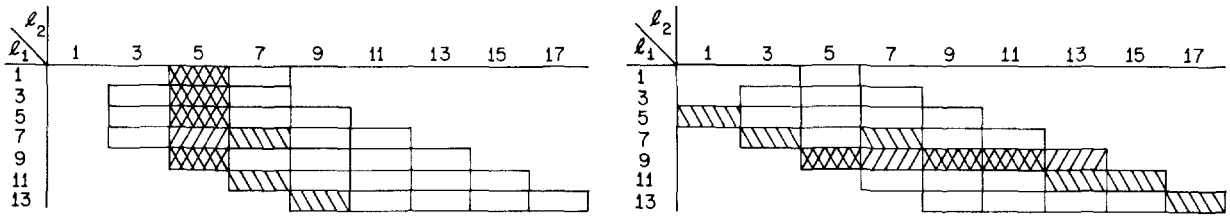

FIG. 5. (a) Model 1 (lines slanted to right) and model 2 (lines slanted to left) applied to a plane of channels in the set for $\psi_{5,5}^{0,9}$. (b) Model 3 (lines slanted to right) and model 4 (lines slanted to left) applied to a plane of channels in the set for $\psi_{5,5}^{0,9}$.

channel or the channel in the plane vertically connected to the initial channel. We will look at just one channel plane for $\psi_{5,5}^{0,9}$, where we will presume that all channels with l_1 equal to 1–13 are needed for completeness. The plane is shown in Figs. 5(a) and 5(b). The four sets of restrictions are:

Model 1: Include those channels whose l_2 equals l_2'. These channels are marked by lines slanted to the right in Fig. 5(a).

Model 2: Consider all the channels with the same value for l_1 to be in a row. Starting from the initial channel, advance from row to row, choosing the one channel in each row which, first, is one of the nearest neighbors to the included channel of the previous row and, second, has a value of l_2 nearest without exceeding the row's average value of l_2. These channels are marked by lines slanted to the left in Fig. 5(a).

Model 3: As in Model 1 with "l_1 equals l_1'" replacing "l_2 equals l_2'" and the results shown in Fig. 5(b).

Model 4: As in Model 2 with the roles of l_1 and l_2 interchanged and the results shown in Fig. 5(b).

Models 1 and 2 emphasize scattering in l_1, while models 3 and 4 emphasize scattering in l_2. As in model 2's description, let us divide each plane of channels into rows indexed by l_1. In a complete channel set calculation, the initial channel may scatter into final channels similar to itself; then the most probable final channel in each row is indexed by l_2 equal to l_2'. Under this assumption, model 1's channel set is an average of the complete channel set over l_2. Another assumption is that the quantum numbers of the initial channel would be "forgotten" during a scattering process in which changes in the quantum numbers are large. Then each row's most probable final channel depends on the size of l_1-l_1'. The final channel's l_2 goes from l_2', when l_1-l_1' is small, to the row's average when l_1-l_1' is large. Under this assumption, model 2's channel set is an average of the complete channel set over l_2. Models 3 and 4 are similarly motivated.

For a realistic IP, the complete channel set of $\psi_{l_2'J}^{\alpha' l_1'}$ is usually considered to be at least all the open channels indexed by J and by l_1 and l_2 whose parities are those of l_1' and l_2'. Should any of our models be applied to the thousands of open channels in the I_2–He system, hundreds of channels would still be left in the incomplete channel sets. However, only channels that the IP couples significantly to a pwfn's initial channel are required in a complete set and this number is always much less than all the open channels. These significant channels can be determined from exploratory calculations and experimental results. For each collision system, we will define the channel sets to which the models are applied.

IV. METHODS

We used two methods to solve the coupled set of equations for the channel coefficients and solution vector of each pwfn. The first method is the propagation method of Gordon[11] with one major modification. This modification is the complete elimination of closed channel coefficients from the calculation at intermediate values of r_2 as the channel coefficients propagate from $r_2=0$ to the asymptotic region. This modification is a direct outgrowth of what Gordon refers to as stabilization and is a general feature of all propagation methods. This modification tends to make the computation time proportional to the cube of the number of open channels rather than the number of open and closed channels. See Appendix A for details. Using the propagation method, we obtained approximately three-place accuracy in any probability (squared amplitude of a solution vector element) greater than 10^{-6}. We tested the accuracy of our solution vectors in two ways. First, a vector's probabilities should sum to 1; our sum values were always one to four decimal places. Second, if P_{mn} is the probability that the initial channel m will scatter into final channel n, then $(P_{mn}-P_{nm})/P_{mn}$ should be zero by time reversal. Our values were always less than 0.05 and usually less than 0.01 for all $P_{mn}>10^{-6}$. In model calculations on the I_2–He system, this accuracy could not be obtained when closed channels were included in a model channel set with 20 or more open channels. For unknown reasons the stabilization procedure described by Gordon failed to prevent the closed channel coefficients from exponentially blowing up as they propagate. We did not pursue this difficulty because of expense and because, as we will later prove, BSA-induced errors in $O_{\alpha' l_1'}^{\alpha}$ for the I_2–He system can

be determined by model and BSA calculations that exclude closed channels.

The second method is analytic and approximate but valid when l_2' is very large. In such cases, the initial channel's scattering is essentially elastic. The scattering is that of potential scattering where the potential is the initial channel's expectation value of the IP. The unknown is the phase shift which is one-half the phase of the only nonzero element in the solution vector. The channel expectation value of our IP is a Lennard-Jones potential. For Lennard-Jones potential scattering when l_2' is large, a valid analytic formula exists.[12] Solution vectors calculated by this analytic method pass smoothly, as a function of l_2', into those calculated by the propagation method.

V. THE H_2–Ar SYSTEM

For this system, we calculate both the partial cross sections $\sigma_{0,3}^0$, $\sigma_{1,3}^1$, $\sigma_{0,3}^1$, and $\sigma_{1,3}^0$ using all four models and the BSA, and the partial differential cross sections $d\sigma_{0,3}^0(\theta_2)$, $d\sigma_{1,3}^1(\theta_2)$, $d\sigma_{0,3}^1(\theta_2)$, and $d\sigma_{1,3}^0(\theta_2)$ using models 1 and 3 and the BSA. To review our notation, $\sigma_{\alpha' l_1'}^{\alpha}$ and $d\sigma_{\alpha' l_1'}^{\alpha}(\theta_2)$ are the cross section and differential cross section, respectively, for the scattering of a randomly oriented diatom in the vibrational rotational state of α' and l_1' into all states with quantum number α. We solve for pwfn's $\psi_{l_2' J}^{0,3}$ and $\psi_{l_2' J}^{1,3}$ for all J and for l_2' ranging from 0 to 199. The propagation method was used for l_2' between 0 and 80 and the analytic method for l_2' between 81 and 199. The models restrict the complete channel sets of $\psi_{l_2' J}^{0,3}$ and $\psi_{l_2' J}^{1,3}$. The range of values that the α, l_1, and l_2 indices of a channel can assume specifies a pwfn's complete channel set. This range may vary with all four indices of the pwfn, but we let it vary only with l_2'. In Table II, the range of α and l_1 as a function of l_2' are listed for the H_2–Ar system. For $l_2'>80$ the channel scattering is essentially elastic and the pwfn's complete channel set is just its initial channel. For each pwfn, l_2 ranges over all values allowed by the pwfn's value of J. Not all open channels are included, but we estimate that use of this channel set would incorrectly determine only vibrationally elastic and inelastic lateral processes of probabilities less than 10^{-4} and 10^{-7}, respectively. $O_{\alpha' l_1'}^{\alpha}$ would probably not be altered by an exact calculation with pwfn channel sets larger than those of Table II.

TABLE II. Range of l_1 as a function of α and l_2' for the complete channel sets of H_2–Ar.

	α		
l_2'	0	1	2
0–40	1, 3, 5	1, 3, 5	1, 3, 5
41–80	1, 3, 5	1, 3, 5	

TABLE III. Partial cross sections in square angstroms for H_2–Ar.

Type	σ	ϵ	$\sigma_{0,3}^0$	$\sigma_{1,3}^1$	$\sigma_{0,3}^1$	$\sigma_{1,3}^0$
Model 1	48.14	0.01158	51.94	65.29	0.000706	0.00225
Model 3	48.14	0.01158	51.94	65.05	0.000725	0.00226
BSA0	48.14	0.01158	51.97	64.94	0.000687	0.00214
BSA1	47.66	0.01158	50.77	63.33	0.000752	0.00234
BSA2	48.62	0.01158	53.18	66.57	0.000628	0.00195
BSA3	48.14	0.01043	50.48	61.24	0.000699	0.00218
BSA4	48.14	0.01273	53.53	68.82	0.000680	0.00211

A. Model 1, Model 3, and the BSA

The full expression[13] for the partial cross section $\sigma_{\alpha' l_1'}^{\alpha}$ is

$$\sigma_{\alpha' l_1'}^{\alpha}=\lambda\!\!\!^{-2}\pi(2l_1'+1)^{-1}\sum_{l_2'=0}^{\infty}\sum_{J=|l_2'-l_1'|}^{l_2'+l_1'}(2J+1)$$

$$\times\sum_{l_1}\sum_{l_2=|J-l_1|}^{J+l_1}|\,\delta_{\alpha' l_1' l_2'}^{\alpha l_1 l_2}-{}^{J}S_{\alpha' l_1' l_2'}^{\alpha l_1 l_2}\,|^2, \quad (7)$$

where $\lambda\!\!\!^{-}$ is the wavelength for the initial translational motion divided by 2π. The sum over l_1 includes all values with the same parity as that of l_1'; δ_i^j is 1 when i equals j and zero otherwise. For each model calculation, the solution vector elements indexing final channels left out of the channel set equal zero in the expression. For a BSA calculation, all vector elements not of the form ${}^{J}S_{\alpha' l_1' l_2'}^{\alpha l_1' l_2'}$ can be set to zero. Furthermore a BSA solution vector is independent of J. Let us represent ${}^{J}S_{\alpha' l_1' l_2'}^{\alpha l_1' l_2'}$ by ${}^{l_1' l_2'}S_{\alpha'}^{\alpha}$ for the BSA calculation. Since

$$(2l_1'+1)^{-1}\sum_{J=|l_2'-l_1'|}^{l_2'+l_1'}(2J+1)=(2l_2'+1), \quad (8)$$

the expression for $\sigma_{\alpha' l_1'}^{\alpha}$ can be simplified for the BSA calculation,

$$\sigma_{\alpha' l_1'}^{\alpha}=\lambda\!\!\!^{-2}\pi\sum_{l_2'=0}^{\infty}(2l_2'+1)\,|\,\delta_{\alpha'}^{\alpha}-{}^{l_1' l_2'}S_{\alpha'}^{\alpha}\,|^2. \quad (9)$$

The partial cross sections for models 1 and 3 are in Table III. Table III also shows the results of five BSA calculations indexed from zero to four. Each one uses different values for σ and ϵ in its IP. Only BSA0 uses the values of σ and ϵ used by models 1 and 3. Table III lists σ and ϵ for each calculation. We want to use Table III to estimate the error due to the BSA in the partial cross sections of the H_2–Ar system. From the five BSA calculations, we can give those errors in terms of the errors in the values of σ and ϵ determined by the BSA calculations that reproduce the cross sections of both models. If there were no errors, BSA0 would reproduce

the results of each model. From the results of Table III, models 1 and 3 estimate that BSA-induced errors for the H_2–Ar system are less than 1% in σ and 10% in ϵ for elastic cross sections and less than 1% or 2% in σ for inelastic cross sections. Also, the BSA results show that inelastic cross sections are extremely insensitive to the value of ϵ.

Partial differential cross sections can also be determined from these seven calculations. The full expression[13] for $d\sigma_{\alpha' l_1'}{}^{\alpha}(\theta_2)$ is

$$d\sigma_{\alpha' l_1'}{}^{\alpha}(\theta_2) = (2\pi)^{-1}\int_0^{2\pi} \chi^2 \frac{\pi}{(2l_1'+1)} \sum_{m_1'=-l_1'}^{l_1'} \sum_{l_1} \sum_{m_1=-l_1}^{l_1} \Big| \sum_{l_2'=0}^{\infty} (2l_2'+1)^{1/2} i^{l_2'} \times \sum_{J=|l_2'-l_1'|}^{l_2'+l_1'} \sum_{M=-J}^{J} \sum_{l_2=|J-l_1|}^{J+l_1} \sum_{m_2=-l_2}^{l_2} i^{-l_2}(l_2' l_1' 0 m_1' \mid l_2' l_1' JM) \times [\delta_{\alpha' l_1' l_2'}{}^{\alpha l_1 l_1} - {}^{J}S_{\alpha' l_1' l_2'}{}^{\alpha l_1 l_2}](l_2 l_1 m_2 m_1 \mid l_2 l_1 JM) Y_{l_2 m_2}(\theta_2, \phi_2) \Big|^2 d\phi_2, \quad (10)$$

where $(ijkl \mid ijmn)$ is a Clebsch–Gordan coefficient and $Y_{l_2 m_2}(\theta_2, \phi_2)$ is a spherical harmonic. Notice our partial cross section is averaged over ϕ_2 space. $\sigma_{\alpha' l_1'}{}^{\alpha}$ and $d\sigma_{\alpha' l_1'}{}^{\alpha}(\theta_2)$ are related by

$$\sigma_{\alpha' l_1'}{}^{\alpha} = 2\pi \int_0^{\pi} d\sigma_{\alpha' l_1'}{}^{\alpha}(\theta_2) \sin\theta_2 d\theta_2. \quad (11)$$

The properties of Clebsch–Gordan coefficients allow $d\sigma_{\alpha' l_1'}{}^{\alpha}$ to be simplified for a BSA calculation,

$$d\sigma_{\alpha' l_1'}{}^{\alpha} = \chi^2 \times \tfrac{1}{4} \Big| \sum_{l_2'=0}^{\infty} (2l_2'+1)[\delta_{\alpha'}{}^{\alpha} - {}^{l_1' l_2'}S_{\alpha'}{}^{\alpha}] P_{l_2'}(\cos\theta_2) \Big|^2. \quad (12)$$

In Figs. 6, 7, 8, and 9, we plot $d\sigma_{0,3}{}^{0}(\theta_2)$, $d\sigma_{1,3}{}^{1}(\theta_2)$, $d\sigma_{0,3}{}^{1}(\theta_2)$, and $d\sigma_{1,3}{}^{0}(\theta_2)$, respectively, for model 1, model 3, and BSA0. In Figs. 10 and 11, we plot $d\sigma_{1,3}{}^{1}(\theta_2)$ and $d\sigma_{0,3}{}^{1}(\theta_2)$, respectively, for BSA1, BSA2, BSA3, and BSA4. In each figure, unless θ_2 is very small, $d\sigma_{\alpha' l_1'}{}^{\alpha}(\theta_2)$ is plotted over those values of θ_2 for which the cross section is large. At very small angles, differential cross sections cannot be measured because of experimental difficulties. Figures 6–11 show two features. First, models 1 and 3 estimate the BSA-induced errors for the H_2–Ar system to be about 1% or 2% in σ for the inelastic partial differential cross sections. Second, the inelastic partial differential cross sections are not sensitive to ϵ and the elastic partial differential cross sections are not sensitive to either ϵ or σ. All the potential sensitivity in elastic differential cross sections is concentrated in the experimentally inaccessible region of very small angles. We confirm this in Table IV, where the values of $d\sigma_{0,3}{}^{0}(\theta_2)$ for θ_2 equal to 0° through 4° are listed for all five BSA calculations. The difference in potential sensitivity of elastic cross sections and elastic differential cross sections are due to experimental limitations. However, the lack of sensitivity to ϵ-like parameters in inelastic cross sections and inelastic differential cross sections are due to the nature of the collision system.

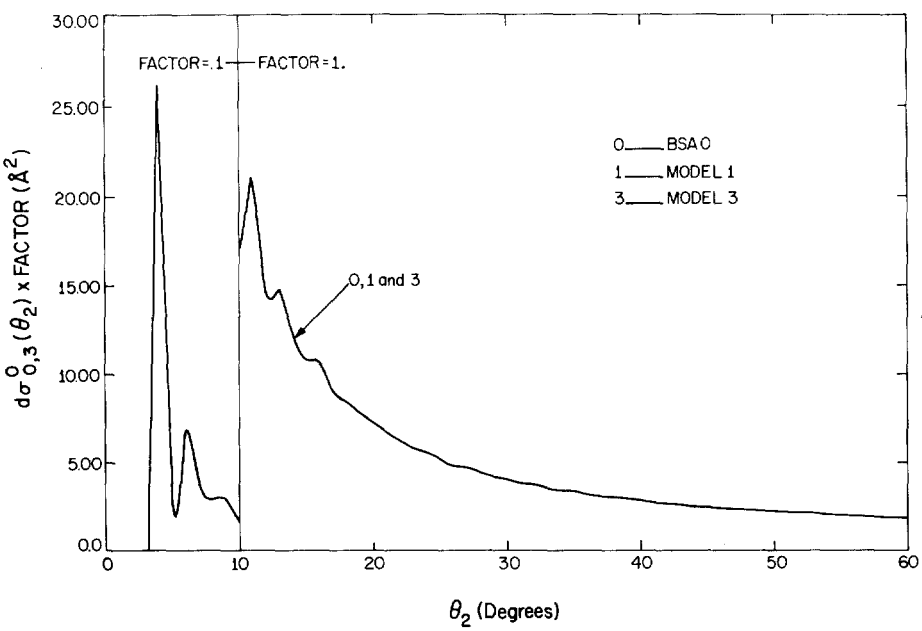

FIG. 6. $d\sigma_{0,3}{}^{0}(\theta_2)$ for H_2–Ar. Each curve is generated from a calculated value at every degree.

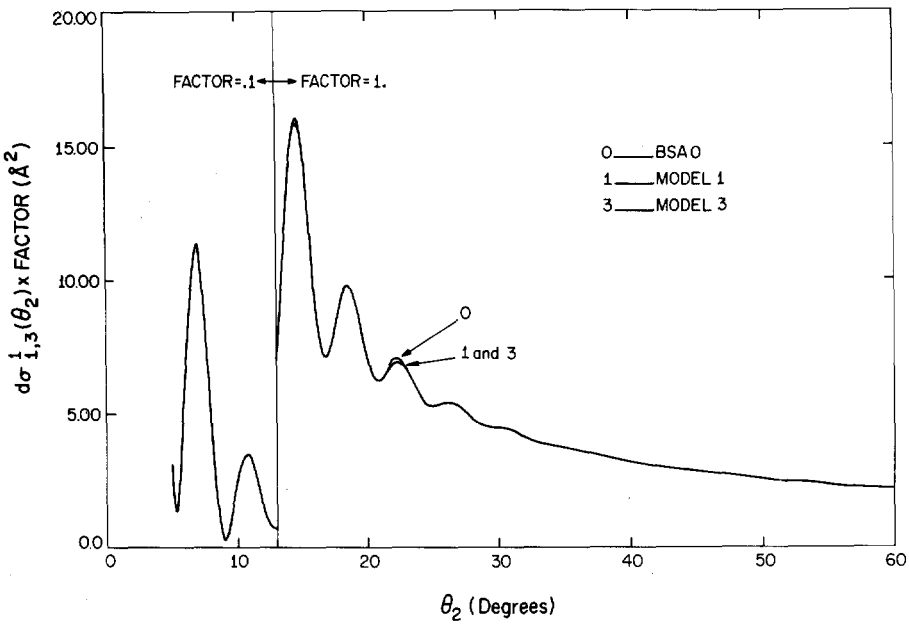

FIG. 7. $d\sigma_{1,3}{}^{1}(\theta_2)$ for H_2–Ar. Each curve is generated from a calculated value at every degree.

B. Interpolation for Partial Cross Sections

Because models 2 and 4 allow more lateral scattering than models 1 and 3, the former are less likely to underestimate errors due to the BSA. They are also much more expensive to use. To circumvent this difficulty, we have devised a way of interpolating, with respect to l_2', the solution vectors of either a model or a BSA calculation. The interpolated vectors are good only for the construction of approximate partial cross sections. However the difference between an approximate cross section of a model and that of a BSA calculation is almost exactly the same as the difference between analogous uninterpolated cross sections. Therefore, the interpolation scheme can be used without destroying the ability of model calculations to determine BSA-induced errors in partial cross sections.

The comparison of Eqs. (7) and (9) shows that both the full and BSA expression for $\sigma_{\alpha' l_1'}{}^{\alpha}$ depends on a sum over l_2'. Each term in the l_2' sum of the BSA expression can be constructed from the solution vector ${}^{l_1' l_2'}\mathbf{S}_{\alpha'}$. The amplitude squared and the phase of each element in this solution vector is a relatively smooth function of l_2'. Each term in the l_2' sum of the full expression can be constructed from solution vectors ${}^{J}\mathbf{S}_{\alpha' l_1' l_2'}$ for all J. The amplitude squared and phase of each element in these vectors is not a smooth function of l_2'. Let us

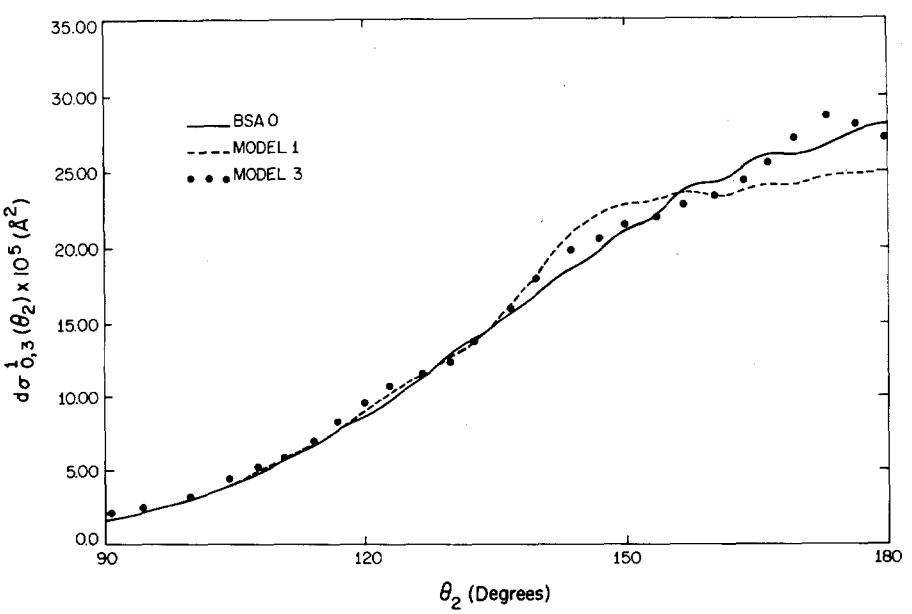

FIG. 8. $d\sigma_{0,3}{}^{1}(\theta_2)$ for H_2–Ar. Each curve is generated from a calculated value at every other degree.

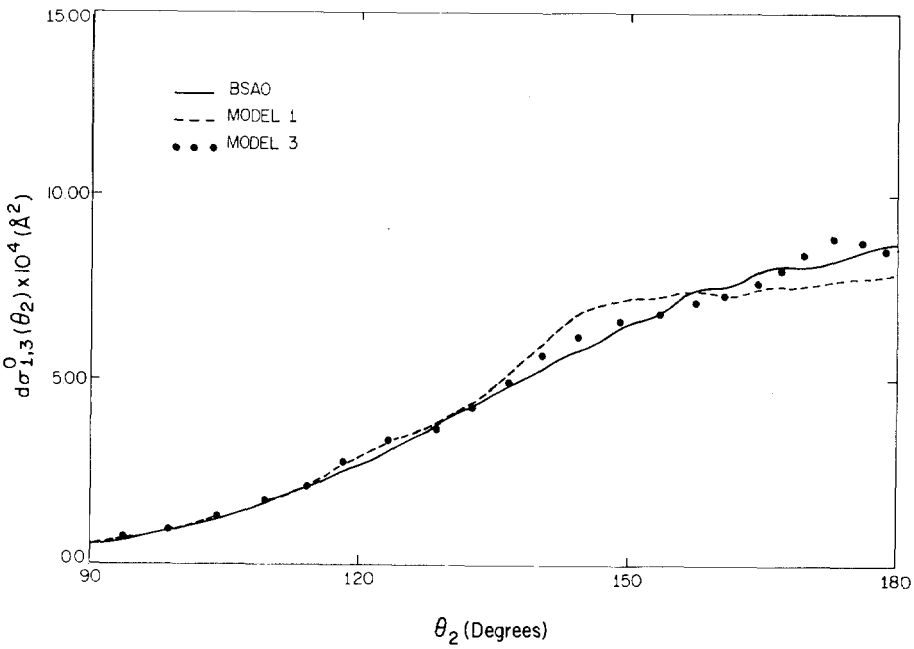

FIG. 9. $d\sigma_{1,3}{}^0(\theta_2)$ for H_2–Ar. Each curve is generated from a calculated value at every other degree.

rearrange the full expression for $\sigma_{\alpha' l_1'}{}^{\alpha}$ into

$$\sigma_{\alpha' l_1'}{}^{\alpha}=\chi^2\pi\sum_{l_2'=0}^{\infty}(2l_2'+1)\times\{|\,\delta_{\alpha'}{}^{\alpha}-{}^{V l_1' l_2'}S_{\alpha'}{}^{\alpha}\,|^2+|\,{}^{L l_1' l_2'}S_{\alpha'}{}^{\alpha}\,|^2\}. \quad (13)$$

We call ${}^{V l_1' l_2'}\mathbf{S}_{\alpha'}$ and ${}^{L l_1' l_2'}\mathbf{S}_{\alpha'}$ vertical and lateral pseudovectors, respectively. To form a term in $\sigma_{\alpha' l_1'}{}^{\alpha}$ for any α we need to know the amplitude squared of each element of both pseudovectors as well as the phase of the elastic element of the vertical pseudovector; these quantities are defined in order as

$$|\,{}^{V l_1' l_2'}S_{\alpha'}{}^{\alpha}\,|^2\equiv[(2l_2'+1)(2l_1'+1)]^{-1}\sum_J(2J+1)\,|\,{}^{J}S_{\alpha' l_1' l_2'}{}^{\alpha l_1' l_2'}\,|^2, \quad (14)$$

$$|\,{}^{L l_1' l_2'}S_{\alpha'}{}^{\alpha}\,|^2\equiv[(2l_2'+1)(2l_1'+1)]^{-1}\sum_J(2J+1)\sum_{l_1}\sum_{l_2}{}_{(l_1,\,l_2)\neq(l_1',\,l_2')}\,|\,{}^{J}S_{\alpha' l_1' l_2'}{}^{\alpha l_1 l_2}\,|^2, \quad (15)$$

$${}^{V l_1' l_2'}\phi_{\alpha'}{}^{\alpha'}\equiv\arccos\left[\frac{[(2l_2'+1)(2l_1'+1)]^{-1}\sum_J(2J+1)\,|\,{}^{J}S_{\alpha' l_1' l_2'}{}^{\alpha' l_1' l_2'}\,|\cos{}^{J}\phi_{\alpha' l_1' l_2'}{}^{\alpha' l_1' l_2'}}{(|\,{}^{V l_1 l_2}S_{\alpha'}{}^{\alpha'}\,|^2)^{1/2}}\right], \quad (16)$$

where ${}^{l}\phi_m{}^{n}$ is the phase of vector element ${}^{l}S_m{}^{n}$. These quantities are all relatively smooth functions of l_2'. To compare BSA and model-determined cross sections, we can calculate BSA solution vectors and model pseudovectors for the same grid of l_2' values, then interpolate with respect to l_2' the remaining vectors and pseudovectors to form the cross sections. If the grid of l_2' values is fine enough to produce approximately correct cross sections, then the differences between these BSA and model cross sections will be nearly exact. Since it is trivial to generate solution vectors or pseudovectors by the analytical method, the interpolation need only be carried out in the region of l_2' where the propagation method applies. Because any phase is undetermined within an integral multiple of 2π, the interpolation of the elastic phases of the solution or pseudovectors is not straightforward; this minor complication is fully discussed in Appendix B.

C. Model 2, Model 4, and the BSA

For the H_2–Ar system, we use our interpolation scheme to determine the partial cross sections for models 2 and 4 and to redetermine the cross sections for models 1 and 3 and the five BSA calculations. For $l_2'=0$–80, we solve for the solution and pseudovectors for every tenth value of l_2', starting from 0, and interpolate the remaining vectors. The results are in Table V. The comparison of Table V to Table III confirms our assertion that the interpolation scheme can produce partial cross sections whose absolute values are approximate, but whose relative values are exact. The

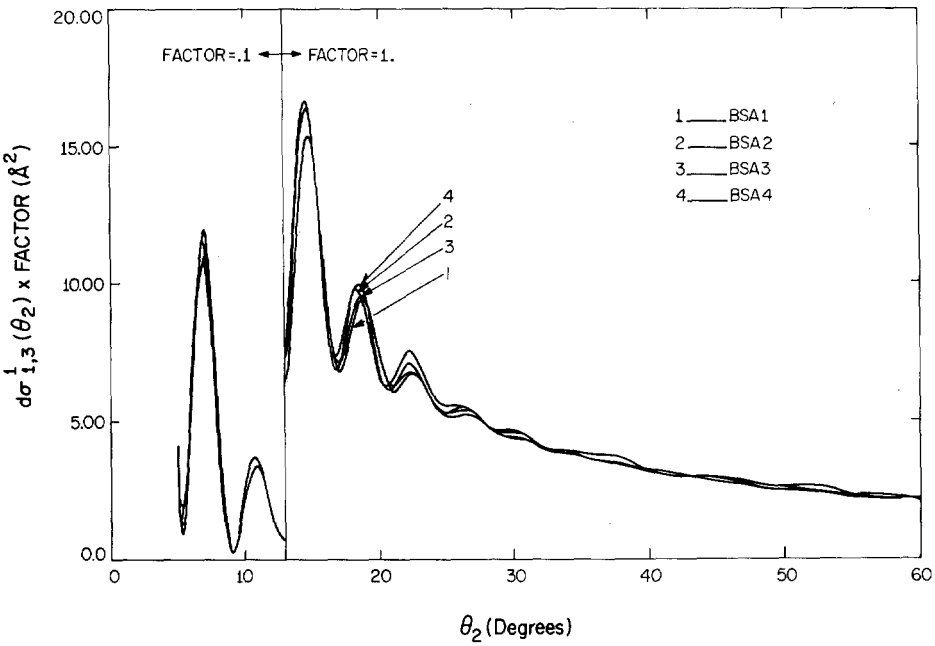

FIG. 10. $d\sigma_{1,3}{}^1(\theta_2)$ for H_2–Ar. Each curve is generated from a calculated value at every degree.

results of Table V show that the BSA-induced errors in partial cross sections are the same for all four models.

All our calculations on the H_2–Ar system support two conclusions:

(1) The BSA can be used to determine accurately the symmetric part of the IP from measurements sensitive to potential parameters.

(2) The inelastic partial cross sections are insensitive to ϵ-like parameters while the entire potential sensitivity of the elastic partial differential cross sections is concentrated in the very small angle region.

VI. THE O_2–He AND I_2–He SYSTEMS

A. Interpolation for Pseudovectors

The construction of ${}^{V}{}_{l_1'l_2'}\mathbf{S}_{\alpha'}$ and ${}^{L}{}_{l_1'l_2'}\mathbf{S}_{\alpha'}$ requires ${}^{J}\mathbf{S}_{\alpha'l_1'l_2'}$ for all J. If $l_2' \geq l_1'$, the number of values for J is $(2l_1'+1)$. For H_2–Ar, $(2l_1'+1)$ is only 7; but for O_2–He and I_2–He, it is 27 and 65, respectively. For model calculations on the O_2–He and I_2–He systems, the number of solution vectors which must be calculated for each pair of pseudovectors is so large that the determination of partial cross sections by the interpolation of pseudovectors is impractical. To overcome this difficulty, we again turn to interpolation. From one solution vector, three quantities are used in the construction of the parts of the two pseudovectors that are used in the expression for the partial cross section. From Eqs. (14)–(16), the three quantities are: $|\,{}^{J}S_{\alpha'l_1'l_2'}{}^{\alpha l_1' l_2'}\,|^2$ for all α,

$$\sum_{\substack{l_1\ l_2 \\ (l_1,\ l_2)\neq(l_1',\ l_2')}} \sum |\,{}^{J}S_{\alpha'l_1'l_2'}{}^{\alpha l_1 l_2}\,|^2$$

for all α, and ${}^{J}\phi_{\alpha'l_1'l_2'}{}^{\alpha'l_1'l_2'}$. These quantities are not smooth functions of J but are relatively smooth functions of ${}^{J}\langle\alpha'l_1'l_2'\,|\,P_2(\cos\gamma)\,|\,\alpha'l_1'l_2'\rangle$ designating the expectation value of $P_2(\cos\gamma)$ with respect to the initial channel ${}^{J}\,|\,\alpha'l_1'l_2'\rangle$. This expectation value contains the entire J dependence of the initial channel's expectation value of our asymmetric IP [see Eq. (3)]. Let us index a model calculation by nJ when each calculated pair of

TABLE IV. $d\sigma_{0,3}{}^0(\theta_2)$ in square angstroms for very small angles for H_2–Ar.

Type	0°	1°	2°	3°	4°
BSA0	18 420	7479	1639	2.26	262
BSA1	17 510	7248	1635	1.09	253
BSA2	19 370	7711	1637	5.39	270
BSA3	16 430	7177	1604	1.04	254
BSA4	20 600	7801	1675	4.87	271

TABLE V. Partial cross sections in square angstroms for H_2–Ar. Cross sections constructed by interpolation.

Type	σ	ϵ	$\sigma_{0,3}{}^0$	$\sigma_{1,3}{}^1$	$\sigma_{0,3}{}^1$	$\sigma_{1,3}{}^0$
Model 1	48.14	0.01158	52.63	61.45	0.000737	0.00235
Model 2	48.14	0.01158	52.66	61.03	0.000822	0.00237
Model 3	48.14	0.01158	52.64	61.25	0.000727	0.00249
Model 4	48.14	0.01158	52.65	61.14	0.000699	0.00252
BSA0	48.14	0.01158	52.65	61.29	0.000712	0.00222
BSA1	47.66	0.01158	51.83	59.37	0.000785	0.00244
BSA2	48.62	0.01158	53.61	63.28	0.000649	0.00202
BSA3	48.14	0.01043	51.43	57.98	0.000732	0.00228
BSA4	48.14	0.01273	54.02	64.44	0.000708	0.00220

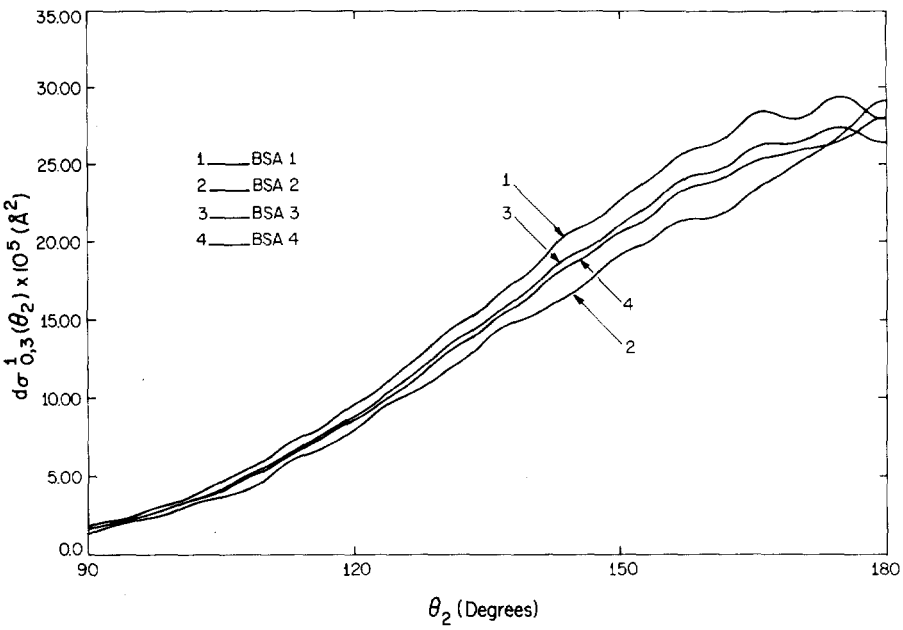

FIG. 11. $d\sigma_{0,3}{}^1(\theta_2)$ for H_2–Ar. Each curve is generated from a calculated value at every other degree.

pseudovectors was constructed from n solution vectors from the propagation method and the remaining solution vectors from interpolation of the above three quantities with respect to ${}^J\langle\alpha' l_1' l_2' \mid P_2(\cos\gamma) \mid \alpha' l_1' l_2'\rangle$. These calculated pairs of pseudovectors are used to interpolate other pseudovectors, with respect to l_2', to form partial cross sections. For a fixed interpolation of pseudovectors with respect to l_2', the interpolation of solution vectors with respect to ${}^J\langle\alpha' l_1' l_2' \mid P_2(\cos\gamma) \mid \alpha' l_1' l_2'\rangle$ is accurate for that value n such that there is a negligible difference in partial cross sections between the nJ and the $(n-1)J$ model calculation. Let us call All-J a model calculation where all solution vectors used in the construction of pseudovectors were calculated; the model calculations for the H_2–Ar system were All-J calculations. In Table VI we compare the partial cross sections for the H_2–Ar system determined by $2J$, $3J$, and All-J calculations of models 2 and 4. Any of the three calculations for both models would have estimated the same degree of BSA-induced error in partial cross sections. This indicates that our interpolation scheme drastically reduces the number of solution vectors that must be calculated for each pair of pseudovectors.

TABLE VI. Partial cross sections in square angstroms for H_2–Ar from the $2J$, $3J$, and All-J calculations of models 2 and 4. Cross sections constructed by interpolation.

Type	$\sigma_{0,3}{}^0$	$\sigma_{1,3}{}^1$	$\sigma_{0,3}{}^1$	$\sigma_{1,3}{}^0$
Model 2 ($2J$)	52.56	61.05	0.000884	0.00242
Model 2 ($3J$)	52.65	61.03	0.000869	0.00240
Model 2 (All J)	52.66	61.03	0.000822	0.00237
Model 4 ($2J$)	52.65	61.16	0.000707	0.00256
Model 4 ($3J$)	52.65	61.14	0.000695	0.00261
Model 4 (All J)	52.65	61.14	0.000699	0.00252

B. Results for the O_2–He System

For this system, we calculate $\sigma_{0,13}{}^0$, $\sigma_{1,13}{}^1$, $\sigma_{0,13}{}^1$, and $\sigma_{1,13}{}^0$ for only model 2 and the BSA. We solve for pwfn's $\psi_{l_2'J}{}^{0,13}$ and $\psi_{l_2'J}{}^{1,13}$ for l_2' ranging from 0 to 130. The propagation method is used for $l_2'=0$, 9, 18, 27, 36, 48, 60, 70, and 80; interpolation with respect to l_2' supplies the missing pseudovectors for $l_2'=0$–80. The analytic method is used for $l_2'=81$–130. The complete channel sets of $\psi_{l_2'J}{}^{0,13}$ and $\psi_{l_2'J}{}^{1,13}$ are defined in Table VII where, as a function of l_2', the ranges of α and l_1 are listed. A channel set's range of l_2 has all values allowed by the value of J of the set's pwfn. Not all open channels are included in each pwfn's channel set, but we estimate that a calculation with this set would incorrectly determine only vibrationally elastic and inelastic lateral processes of probabilities less than 10^{-4} and 10^{-7}, respectively.

Table VIII lists the partial cross sections for a $2J$ and a $3J$ model 2 calculation and for five BSA calculations. Each BSA calculation uses different values for

TABLE VII. Range of l_1 as a function of α and l_2' for the complete channel sets of O_2–He.

	α		
l_2'	0	1	2
0–36	5, 7, ···, 21	5, 7, ···, 21	7, 9, ···, 19
37–80	5, 7, ···, 21	5, 7, ···, 21	

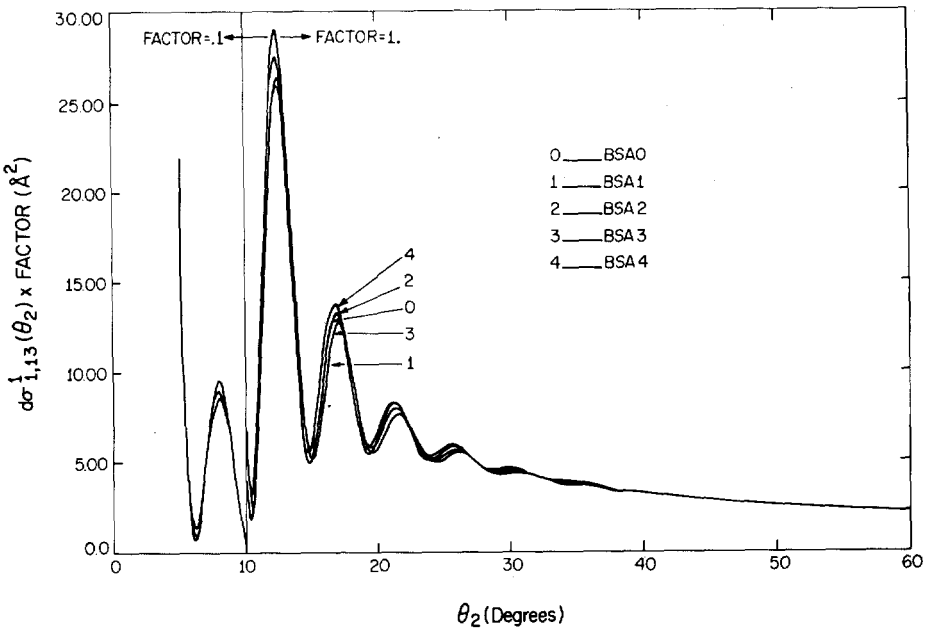

FIG. 12. $d\sigma_{1,13}{}^1(\theta_2)$ for O_2–He. Each curve is generated from a calculated value at every degree.

TABLE VIII. Partial cross sections in square angstroms for O_2–He. Cross sections constructed by interpolation.

Type	σ	ϵ	$\sigma_{0,13}{}^0$	$\sigma_{1,13}{}^1$	$\sigma_{0,13}{}^1$	$\sigma_{1,13}{}^0$
Model 2 (2J)	115.5	0.01593	52.87	61.45	0.00326	0.00927
Model 2 (3J)	115.5	0.01593	52.85	61.47	0.00320	0.00920
BSA0	115.5	0.01593	52.75	60.98	0.00339	0.00980
BSA1	114.3	0.01593	52.53	60.77	0.00363	0.01050
BSA2	116.7	0.01593	53.26	61.60	0.00316	0.00915
BSA3	115.5	0.01433	51.66	58.39	0.00338	0.00978
BSA4	115.5	0.01753	54.02	63.99	0.00340	0.00984

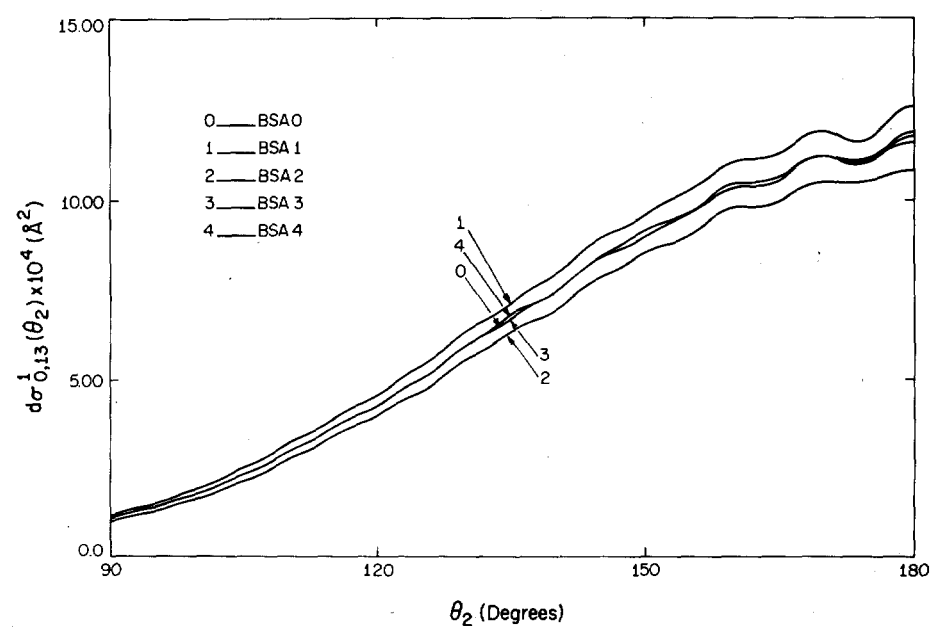

FIG. 13. $d\sigma_{0,13}{}^1(\theta_2)$ for O_2–He. Each curve is generated from a calculated value at every other degree.

TABLE IX. Range of l_1 as a function of α and l_2' for the complete channel sets of I_2–He.

	α	
l_2'	0	1
0–16	22, 24, ···, 46	22, 24, ···, 46
17–24	24, 26, ···, 46	26, 28, ···, 44
25–32	26, 28, ···, 42	26, 28, ···, 42
33–64	26, 28, ···, 38	26, 28, ···, 38

σ and ϵ, which are also listed in Table VIII. From the results of Table VIII, the $2J$ and $3J$ calculations of model 2 are nearly the same and indicate that BSA-induced errors for the O_2–He system are less than 1% in σ and about 5% in ϵ for elastic cross sections and about 1% in σ for inelastic cross sections. The BSA calculations also show that inelastic cross sections are very insensitive to the value of ϵ. Because all four models estimate the same BSA-induced errors in the H_2–Ar system, we doubt that other model calculations on O_2–He would radically alter our conclusions. If we assume that the BSA is as good for differential cross sections as for cross sections, then we can use the BSA to investigate the potential sensitivity of differential cross sections. The five BSA calculations were redone with each solution vector explicitly calculated. In Figs. 12 and 13 we plot $d\sigma_{1,13}{}^1(\theta_2)$ and $d\sigma_{0,13}{}^1(\theta_2)$, respectively, for the five redone BSA calculations. The two figures show that, for O_2–He as for H_2–Ar, the potential sensitivity of the elastic differential cross sections is concentrated in the very small angle region, while the inelastic differential cross sections have the same potential sensitivity as inelastic cross sections.

C. Results for the I_2–He System

For this system, we calculate $\sigma_{0,34}{}^0$, $\sigma_{1,34}{}^1$, $\sigma_{0,34}{}^1$, and $\sigma_{1,34}{}^0$ for only model 2 and the BSA. We solve for pwfn's $\psi_{l_2'J}{}^{0,34}$ and $\psi_{l_2'J}{}^{1,34}$ for l_2' ranging from 0 to 100. The propagation method is used for every eighth value of l_2' from 0 to 64; interpolation with respect to l_2' supplies the missing pseudo vectors for $l_2'=0$ to 64. The analytic method is used for $l_2'=65$ to 100. The complete channel sets of $\psi_{l_2'J}{}^{0,13}$ and $\psi_{l_2'J}{}^{1,13}$ are defined in Table IX where, as a function of l_2', the ranges of α and l_1 are listed. A channel set's range of l_2 has all values allowed by the value of J of the set's pwfn. Due to the technical difficulties discussed in Sec. IV, the channel sets defined by Table IX have no closed channels. We will discuss the effect of their absence on partial cross sections. We estimate that the absence of some open channels from the channel sets of Table IX will affect only vibrationally elastic and inelastic lateral processes of probabilities less than 10^{-4} and 10^{-5}, respectively.

TABLE X. Partial cross sections in square angstroms for I_2–He. Cross sections constructed by interpolation. No closed channels used in calculations.

Type	σ	ϵ	$\sigma_{0,34}{}^0$	$\sigma_{1,34}{}^1$	$\sigma_{0,34}{}^1$	$\sigma_{1,34}{}^0$
Model 2 ($2J$)	128.3	0.4073	424.4	440.2	1.058	2.627
Model 2 ($3J$)	128.3	0.4073	424.0	440.7	1.054	2.618
BSA0	128.3	0.4073	424.1	431.2	1.063	2.598
BSA1	125.7	0.4073	412.8	385.7	1.058	2.587
BSA2	130.9	0.4073	430.3	480.7	1.065	2.603
BSA3	128.3	0.3870	428.8	416.4	1.001	2.446
BSA4	128.3	0.4275	418.3	457.4	1.126	2.752

Table X lists the partial cross sections for a $2J$ and a $3J$ model 2 calculation and for five BSA calculations for five different values of σ and ϵ. From the results of Table X, the $2J$ and $3J$ calculations of model 2 are nearly the same and indicate that BSA induced errors for the I_2–He system are less than 1% in σ and 5% in ϵ for the elastic cross sections and less than 5% in ϵ for the inelastic cross sections. The BSA calculations also show that inelastic cross sections are insensitive to the value of σ. To determine the effect on partial cross sections of the absence of closed channels from all channel sets, we redid the five BSA calculations including two closed channels in each pwfn's channel set. The resulting partial cross sections are listed in Table XI. The elastic cross sections are unchanged; the inelastic cross sections are all changed by the same small amount, leaving their relative values unchanged. We believe model cross sections will undergo the same alternations if closed channels are used in the calculation. By assuming the BSA is equally good for cross sections and differential cross sections, we redid once again the five BSA calculations to investigate the potential sensitivity of differential cross sections. In this new set of calculations, closed channels were used and each solution vector was explicitly calculated. In Fig. 14 we plot $d\sigma_{1,34}{}^1(\theta_2)$ for three BSA calculations and in Fig. 15 we plot $d\sigma_{0,34}{}^1(\theta_2)$ for all five BSA calculations. The two figures show that the elastic and inelastic differential cross sections of I_2–He have size and structure over a far wider range of angles than the differential cross sections of H_2–Ar and O_2–He. The large values of σ and ϵ make the collision of He and I_2 much "stickier" than the collision of Ar with H_2 or of He with O_2. Large-angle scattering is significant with the consequence that both the inelastic

TABLE XI. Partial cross sections in square angstroms for I_2–He. Cross sections constructed by interpolation. Closed channels used in calculations.

Type	$\sigma_{0,34}{}^0$	$\sigma_{1,34}{}^1$	$\sigma_{0,34}{}^1$	$\sigma_{1,34}{}^0$
BSA0	424.0	431.1	1.091	2.666
BSA1	412.8	385.0	1.087	2.658
BSA2	430.3	480.3	1.091	2.667
BSA3	428.8	410.9	1.026	2.509
BSA4	418.0	457.7	1.156	2.825

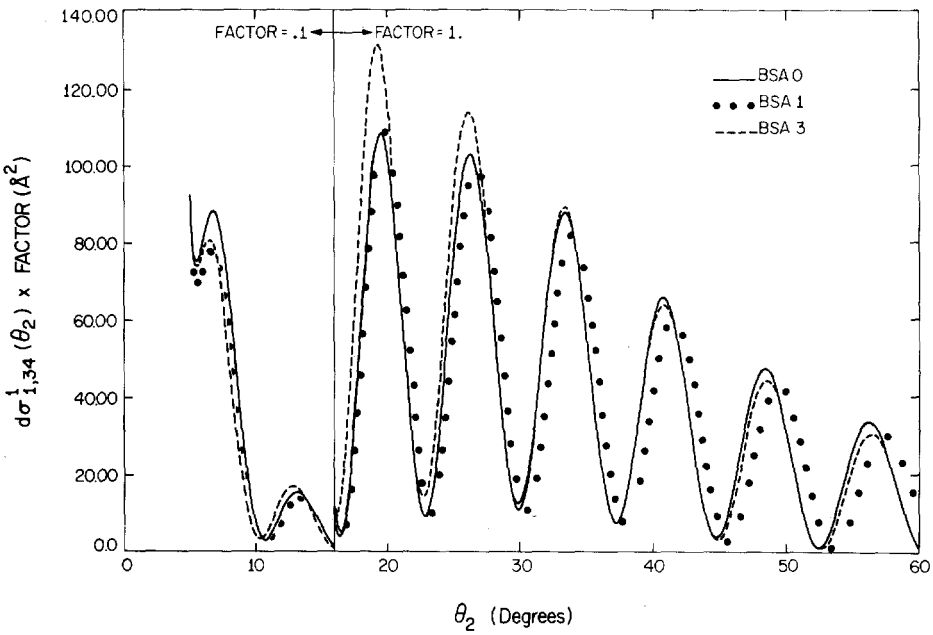

FIG. 14. $d\sigma_{1,34}{}^1(\theta_2)$ for I_2–He. Each curve is generated from a calculated value at every degree.

and elastic *differential* cross sections of I_2–He show the same potential sensitivity as the corresponding cross sections.

VII. CONCLUSIONS

Two conclusions about low-energy vibrational scattering in homonuclear diatom–atom collisions can be drawn from our results for the H_2–Ar, O_2–He, and I_2–He systems. First, the breathing sphere approximation can be used to analyze accurately experimental measurements for the potential parameters to which the measurements are sensitive. Second, the measurements most sensitive to potential parameters are, first, elastic cross sections, and, second, inelastic cross sections and inelastic differential cross sections. Elastic differential cross sections are as sensitive as elastic cross sections if the intermolecular potential is soft and the collision is "sticky" with large-angle scattering (like I_2–He). Otherwise the entire potential sensitivity of elastic differential cross sections will be concentrated in the experimentally difficult region of very small angle scattering.

The approach used in this work can be applied to the study of the orientation effect of strong dipole forces present in most heteronuclear diatom–atom vibrational scattering. The intermolecular potential used in a

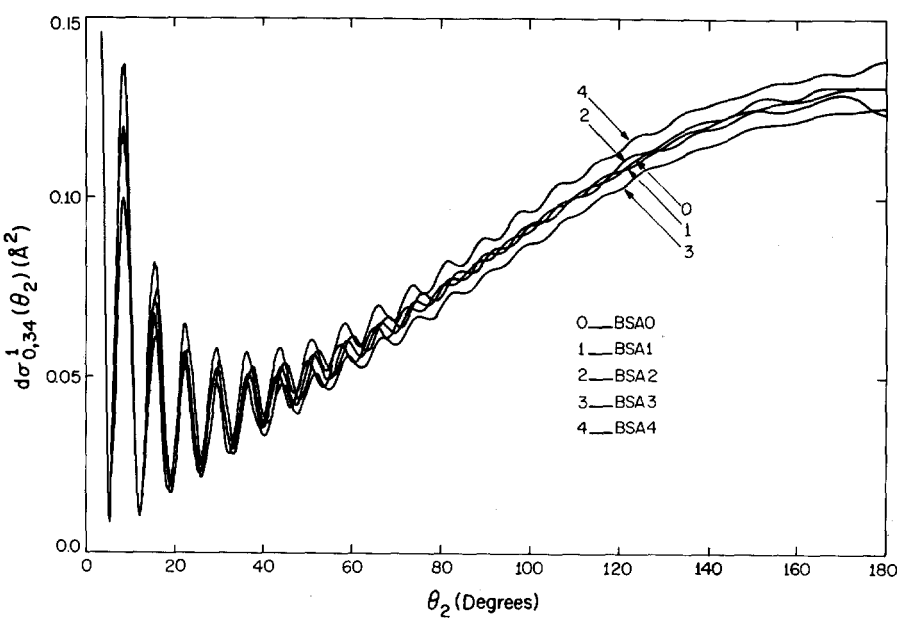

FIG. 15. $d\sigma_{0,34}{}^1(\theta_2)$ for I_2–He. Each curve is generated from a calculated value at every other degree.

breathing-sphere-approximation calculation cannot align the atom and diatom during collision, whereas the intermolecular potential used in a model calculation can. A significant difference between BSA and model observables would indicate the aligning power of dipole forces significantly affects vibrational scattering.

ACKNOWLEDGMENT

We thank Dr. Robert J. Gordon for helpful discussions and the use of his JWKB phase shift computer program.

APPENDIX A

The coupled set of differential equations for the channel coefficients of an expanded partial wavefunction (pwfn) can be formulated in terms of matrix operators and vector solutions. Only the particular vector solution which obeys the correct boundary conditions [see Eq. (6) and following text] is a set of channel coefficients. For an expansion set of N channels, let us define an $N\times N$ matrix ϕ whose Lth column, for $L=1, \cdots, N$, is the set of channel coefficients for the expanded pwfn whose initial channel is indexed by L. To obtain a column of ϕ, either a matrix[14] or a propagation[15] approach must be used. Both approaches calculate an $N\times N$ matrix ψ whose columns are vector solutions which obey boundary conditions different from those of channel coefficients,

$$\psi_{ij}(r_2) \underset{r_2\to 0}{\longrightarrow} 0 \qquad \text{(matrix or propagation)}, \tag{A1}$$

$$(\partial/\partial r_2)\psi_{ij}(r_2) \underset{r_2\to 0}{\longrightarrow} A_{ij} \qquad \text{(propagation)}, \tag{A2}$$

$$\psi_{ij}(\bar{r}_2) = B_{ij} \qquad \text{(matrix)}, \tag{A3}$$

where $\bar{r}_2$ is in the asymptotic region. $\mathbf{A}$ and $\mathbf{B}$ are arbitrarily chosen constant matrices whose elements are A_{ij} and B_{ij}. If $\mathbf{A}$ or $\mathbf{B}$ are linearly independent, ψ, like ϕ, will be composed of N linearly independent vector solutions. Since there are only N channels in the expansion, both ψ and ϕ span the space of vector solutions. Consequently, there exists a matrix $\mathbf{C}$ with a well-defined inverse such that

$$\psi = \phi\mathbf{C}, \tag{A4}$$

$$\phi = \psi\mathbf{C}^{-1}. \tag{A5}$$

Since the form of ϕ in the asymptotic region is specified by the boundary conditions, once ψ is known in the asymptotic region, $\mathbf{C}^{-1}$ and hence ϕ can be readily determined.

From Eq. (A5) it would appear that all N columns of ψ must be calculated to obtain any column of ϕ. This is not true if there are closed channels in the expansion set. Let N_0 be the number of open channels; let a vector solution be open if its closed elements asymptotically approach zero. By the proper choice of B,[14] any matrix method can generate only N_0 columns of ψ which span the space of open vector solutions. Therefore, only the N_0 columns of ψ are needed to obtain any open column of ϕ. Of course, only the open columns of ϕ are physically meaningful.

It is not generally recognized that any propagation method can determine the open columns of ϕ without propagating the full ψ matrix into the asymptotic region. In order to describe how this can be done, we must first discuss several characteristics of ϕ. While we are propagating ψ, we can know nothing of the value of ϕ. However, it is possible to determine several general characteristics of ϕ as a function of r_2. Since ϕ is related to ψ by only a constant matrix $\mathbf{C}$, the characteristics of ϕ can explain some of the propagational behavior of ψ. If there are closed channels, the closed elements of the open columns of ϕ go to zero as r_2 grows large. The physical reason for the behavior is that the collision at large r_2 contains no component of the highly excited motion which closed channels describe. In general, the more highly excited the motion described by the closed channel, the more rapidly its channel coefficient will go to zero as a function of r_2. In general, all closed channel coefficients assume their asymptotic form at values of r_2 smaller than those at which open channel coefficients assume their final form. The closed elements of the closed columns of ϕ go asymptotically to zero relative to the diagonal elements, which grow without limit; since the diagonal element in a closed column refers to the channel coefficient for the initial *closed* channel, it has an exponential growing source term instead of the oscillating one for initial *open* channels. With these features of ϕ in mind, we will now discuss the stabilization of ψ and its implications.

If $\mathbf{A}$ is linearly independent, ψ at the start of its propagation will also be linearly independent. However, due to the unbounded growth of the closed columns of ϕ, at large enough r_2 the closed columns of ϕ will completely dominate $\phi\mathbf{C}$. This means that during propagation each of ψ's columns become, to all the significant figures retained, the linear combination of only the closed columns of ϕ. In other words, when closed channels are present, ψ has an innate tendency to linear dependence. Any procedure which suppresses this tendency we will call stabilization. Although there are several stabilization procedures, their derivations are similar to the following simplified set of arguments. When ψ has propagated to a large enough value of r_2 to show signs of linear dependence, we wish to find a matrix $\mathbf{T}$ which back-multiplies ψ so that $\psi\mathbf{T}$ has a much reduced tendency to linear dependence. Then the propagation is continued with $\psi\mathbf{T}$. The proper $\mathbf{T}$ must remove most of the contribution of the Lth closed column of ϕ from all but the Lth column of $\psi\mathbf{T}$. If the closed elements of ϕ assumed their asymptotic form for all values of r_2, then *all* of the contribution of the Lth closed column of ϕ would be removed from all but the

Lth column of $\psi\mathbf{T}$ if

$$(\psi\mathbf{T})_{LK}=0, \quad \text{for} \quad L\neq K$$
$$=1, \quad \text{for} \quad L=K \qquad \text{(A6)}$$

for all K and for all $L>N_0$. This condition is sufficient to define $\mathbf{T}$. Since ϕ's closed elements do not assume their asymptotic form for all values of r_2, $\mathbf{T}$ defined by Eq. (A6) will leave in each column of $\psi\mathbf{T}$ residual contributions from the closed columns of ϕ. At some larger value of r_2, linear dependence will again appear in $\psi\mathbf{T}$ and the process must be repeated. However, each succeeding transformation leaves fewer and fewer residual contributions from the closed columns of ϕ. In this way a linearly independent ψ can be propagated into the asymptotic region.

Stabilization has two important implications. First, each succeeding transformation makes the first N_0 columns of ψ look like just a linear combination of the open columns of ϕ and makes any other column of ψ look like the corresponding column in ϕ. Consequently, in the asymptotic region, to a high degree of accuracy only the first N_0 columns of ψ are needed to determine any open column of ϕ by Eq. (A5). The only reason for calculating the N_0+1 to N columns of ψ is to permit stabilization; these columns are required in the determination of each $\mathbf{T}$. The second implication of stabilization is as follows. Since each transformation of ψ increases the similarity of its closed rows to those of ϕ, at large enough values of r_2, the nondiagonal elements of each closed row of ψ can be set to its asymptotic form of zero with no appreciable effect on the other elements. In general, this will occur at values of r_2 before the asymptotic region. If a value of r_2 has been reached where the Lth closed row of ψ can be set to zero except for ψ_{LL}, then there is no longer any reason to calculate the Lth column of ψ for it is no longer needed to determine any subsequent $\mathbf{T}$ matrix. In fact, the Lth row and column of ψ can be dropped for the rest of the propagation. In other words, the stabilizing transformations allow the dimensions of ψ to be reduced from $N\times N$ to $N_0\times N_0$ during the course of the propagation. This reduction in the amount of calculation is a feature of the propagation approach analogous to the previously discussed reductions possible with the matrix approach.

In our calculations we use Gordon's propagation method.[11] Before propagating over each step in r_2, we stabilize ψ. After propagating over each step, we form

$$\frac{|(dU_{N_0\bar{N}}/dr_2)\psi_{\bar{N}N_0}|}{|(U_{N_0N_0}-2\epsilon_{N_0}+E)[|\psi_{N_0N_0}|+|(\partial/\partial r_2)\psi_{N_0N_0}|]|},$$

where $\bar{N}\times\bar{N}$ are the effective dimensions of ψ for that step, where $\mathbf{U}$ and its derivative are defined by Gordon, and where ϵ_{N_0} is the energy of the diatomic state factor of the N_0th channel. When this ratio becomes less than 10^{-5}–10^{-8} (depending on the system and the accuracy desired), the $\bar{N}$th row and column are eliminated from ψ and $\bar{N}$ is reduced by 1. Stabilization and this test are continued until $\bar{N}$ is reduced to N_0. The calculation time varies from N^3 to N_0^3 depending on how far out each closed row in ψ must be propagated. For most collisions we have studied, including many not reported in this article, the time has varied more as N_0^3 than N^3, resulting in a significant reduction in calculation costs.

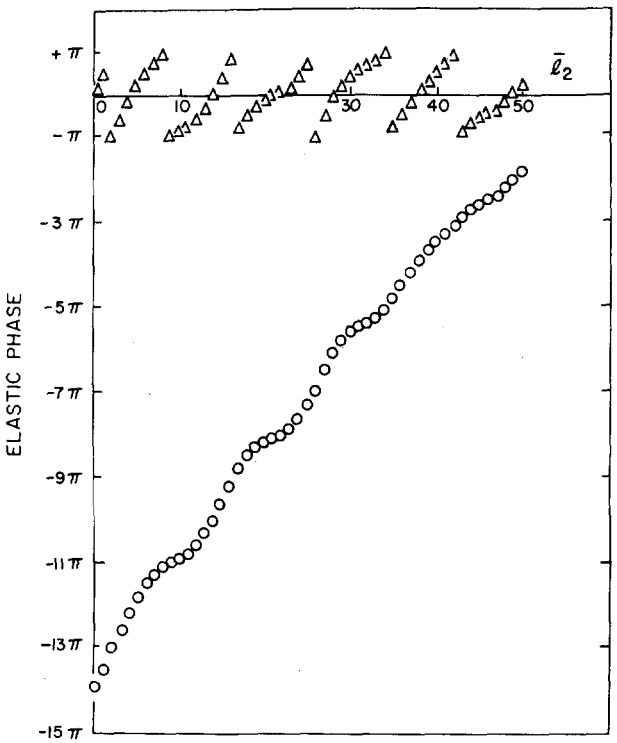

FIG. 16. Elastic phase as a function of l_2'. Phase generated by propagation method (△); phase as a smooth function (○).

APPENDIX B

The elastic phases of solution or pseudovectors are undetermined within an integral multiple of 2π. The propagation method internally adds or subtracts 2π units to its phases to bring them within $\pm\pi$. Figure 16 is the plot of the phase, as both a smooth function of l_2' and as produced by the propagation method. Because the phase as a smooth function of l_2' passes outside the range of $\pm\pi$, the phases produced by the propagation method are not suitable for interpolation with respect to l_2'. For BSA calculations this difficulty can be avoided by using the JWKB method to determine the elastic phase of each solution vector under the gross approximation that the initial channel experiences only potential scattering. The JWKB phases are smooth functions of l_2'. We use these phases to determine the number of 2π units the exact elastic phase of the propagation method must be displaced, by demanding the displaced

phase to be as close as possible to the JWKB phase. The displaced elastic phases are smooth functions of l_2' and are suitable for interpolation. For the pseudoelastic phases of a model calculation, we use the same displacements determined for the BSA calculation whose IP is the symmetric part of the model's IP. In all cases where this procedure was used, the difference between an exact undisplaced and a JWKB phase was, within 1% or 2%, an exact multiple of 2π.

* Alfred P. Sloan Foundation Fellow.
† Contribution No. 4331.

[1] For a survey of such experiments, see R. G. Gordon, W. Klemperer, and J. I. Steinfeld, Ann. Rev. Phys. Chem. **19,** 215 (1968).
[2] For review of theoretical calculations of $O^{\alpha}/\alpha' l_1'$, see Ref. 1; J. L. Stretton, *Transfer and Storage of Energy by Molecules* (Wiley, New York, 1969), Vol. 2, Chap. 2, p. 58; D. Rapp and T. Kassal, Chem. Rev. **69,** 61 (1969).
[3] S. W. Benson and G. C. Berend, J. Chem. Phys. **44,** 4247 (1966).
[4] R. Razner, J. Chem. Phys. **51,** 5602 (1969).
[5] For example, see the calculated Li^+–H_2 IP of W. A. Lester, Jr., J. Chem. Phys. **54,** 3171 (1971).
[6] D. Secrest and B. R. Johnson, J. Chem. Phys. **45,** 4556 (1966).
[7] J. H. Kiefer and R. W. Lutz, J. Chem. Phys. **44,** 668 (1966) and **45,** 3888 (1966).
[8] D. R. White and R. C. Millikan, J. Chem. Phys. **39,** 1807 (1963).
[9] J. I. Steinfeld and W. Klemperer, J. Chem. Phys. **42,** 3475 (1965).
[10] A. M. Arthurs and A. Dalgarno, Proc. Roy. Soc. (London) **256,** 540 (1960).
[11] R. G. Gordon, J. Chem. Phys. **51,** 14 (1969).
[12] N. F. Mott and H. S. W. Massey, *The Theory of Atomic Collisions* (Oxford U. P., New York, 1965), 3rd ed., p. 89.
[13] J. M. Blatt and L. C. Biedenharn, Rev. Mod. Phys. **24,** 258 (1952).
[14] For examples, see V. P. Gutschick, V. McKoy, and D. J. Diestler, J. Chem. Phys. **52,** 4807 (1970); A. S. Cheung and D. J. Wilson, J. Chem. Phys. **51,** 3449, 4733 (1969).
[15] For examples, see Refs. 11 and 6.